Research Article / Review Article FUPRE JOURNAL 10(1):18-34(2025)
https://doi.org//10.60787/FJSIR.v10i1.18-34

FUPRE Journal
of
Scientific and Industrial Research

ISSN: 2579-1184(Print) ISSN: 2578-1129 (Online)

http://fupre.edu.ng/journal

Modeling and Simulation of Solar Energy Harvesting for Reliable Wireless Sensor Node Operation Using Empirical Irradiance Data

***IGBINOBA, C. K.*[1,*], *OKHAIFOH, J. E.*[2]**

[1,2] *Department of Electrical And Electronics Engineering, Federal University Of Petroleum Resources, Nigeria.*

ARTICLE INFO

Received: 01/02/2026
Accepted: 10/05/2026

Keywords

DC–DC converter, Photovoltaic systems, Power management system, Solar energy harvesting, Wireless Sensor Node.

ABSTRACT

This paper presents the modeling and simulation of a solar energy harvesting system analyzed using MATLAB/Simulink under varying seasonal conditions. The proposed architecture consists of a photovoltaic (PV) source, a DC–DC power conversion stage, MPPT controller, a power management system (PMS), storage and a wireless sensor node. A comprehensive monthly comparative analysis was conducted to evaluate converter output power, regulated load power, harvested daily energy, and overall system efficiency. Simulation results demonstrate strong seasonal dependence of harvested energy, with peak production occurring in high-irradiance months up to approximately 4.6 Wh/day, and minimum output during low-irradiance periods approximately 2.3 - 2.5 Wh/day. Despite significant variations in input solar resource, the overall system efficiency remains nearly constant at approximately 7.15% throughout the year, indicating stable converter operation and robust power conditioning. Seasonal aggregation shows that late-year months yield the highest average energy, while mid-year months gives lower operational. Comparative best- and worst-case analysis confirms that performance variations are primarily driven by solar availability rather than internal conversion losses. The results validate the reliability, scalability, and environmental adaptability of the proposed solar energy harvesting system for low-power standalone applications.

1. INTRODUCTION

We are entering the Internet of Things (IoT) era where one of the most important thing is wireless sensor networks (Gubbi *et al*., 2013; Diaz *et al*., 2016; Ray, 2018; Jaehoon *et al*., 2019). Wireless sensor networks (WSNs) consist of numerous sensing devices to collect data and communicate with each other (Ray, 2018). A large number of sensors such as temperature sensors (Ramakrishnan *et al*, 2016)), ultrasonic sensors (Li *et al*., 2018), proximity sensors (Servent *et al*., 2017), or gas sensors (Yamazoe, 2005; Song *et al*., 2017), are widely distributed in the IoT system, and can be operated with wired or wireless power source (Jaehoon *et al*., 2019).

In spite of the significant benefits and widespread applications of WSNs, one of the well-known majors challenged faced with WSNs is limited power supply to sensor node (Shaikh *et al*., 2015; Ahmad *et al*., 2019; Iftikhar *et al*., 2021; Divyanshu *et al*., 2024). The key necessity of a WSNs is that it should be self-sufficient, operate for a particular time, and require little maintenance which can be costly and inconvenient depending on the number of nodes and the application itself which could

*Corresponding author, e-mail: charleskevwe@gmail.com, okhaifoh.joseph@fupre.edu.ng
https://doi.org/10.60787/FJSIR.v10i1.18-34
©Scientific Information, Documentation and Publishing Office at FUPRE Journal

necessitate nodes with limited accessibility (Panatik *et al*., 2016). The major existing power source used by WSNs is battery, but many problems are linked with batteries (Raquid *et al*., 2016). First, severe weather conditions may cause failure on the batteries, resulting in chemical leakages that can cause various environmental problems (Tiliute, 2007). Secondly, batteries are inadequate in providing enough energy for long term applications, which lead to inconvenient frequent charging or replacement (Panella *et al*., 2009; Katrina *et al*., 2021). Finally, for WSNs deployed in areas that are inaccessible, the replacement or recharging of depleted batteries is not feasible, so the device must be designed to ensure that the energy provided by battery is enough for the system's entire anticipated lifecycle (Sichitiu and Dutta, 2005; Abd Aziz *et al*., 2012). A possibility is to use higher capacity batteries to ensure the required power constraints are met, but this result in increased size for the device that is often not acceptable (Marco, 2021).

Though the power efficiency and expected lifetime of WSNs has increased over the last few years due to sensor and software optimizations, lightweight communication protocols, and low-power radio transceivers, power supply remains a major challenge with WSNs (Keh *et al*., 2011; Prauzek *et al*., 2018; Zhou *et al*., 2019; Wang *et al*., 2019).

Energy harvesting has developed as a promising solution to address the energy constraints in WSNs (Choudhary *et al*., 2020; Fadoua and Adil, 2022; Hussain *et al*., 2024; Muhammad *et al*., 2025. By capturing ambient energy from the environment and external sources and converting it into useful electrical energy, sensor nodes can potentially achieve a sustainable power supply (Jaspreet *et al*., 2020).

2. METHODOLOGY

This study adopts a systematic approach that integrates data acquisition, system modeling, and simulation to evaluate the performance of the solar energy harvesting system.

2.1 Experimental Data Collection

The data used in this study was obtained from the NASA POWER project database, which provides reliable and validated meteorological and solar resource data for research from the Federal University of Petroleum Resources, Effurun, Nigeria, located at approximately 5.65°N and 5.62°E. The dataset covers a full year from January 2025 to December 2025, ensuring that both dry and rainy seasonal variations are captured. Solar irradiance data was collected at 20-minute intervals to provide high temporal resolution and accurately reflect daily fluctuations in solar energy. The data was selected to represent real environmental conditions of the study area and to enable realistic simulation and performance evaluation of the solar energy harvesting system.

2.2 System Architecture

The architecture of the solar energy harvester is given in Figure 1. It consists of the solar harvester, buck DC-DC converter, Maximum power point tracking (MPPT) controller, power management system, battery storage and a wireless sensor node.

The solar harvester (photovoltaic panel) converts incident solar radiation into electrical energy, though its output varies due to environmental conditions. To maximize energy extraction, an MPPT (Maximum Power Point Tracking) controller continuously adjusts the operating point of the panel to ensure it delivers peak power. The extracted energy is then conditioned by a buck DC-DC converter, which steps down and regulates the voltage to a stable level suitable for system operation. The regulated power is managed by the Power Management System (PMS), which serves as the control unit by overseeing energy distribution,

battery charging, and load management to ensure efficient utilization. The battery acts as an energy storage element, storing excess energy during periods of high generation and supplying power when solar input is insufficient. Finally, the wireless sensor node represents the load, receiving controlled and reliable power to perform sensing, processing, and communication tasks.

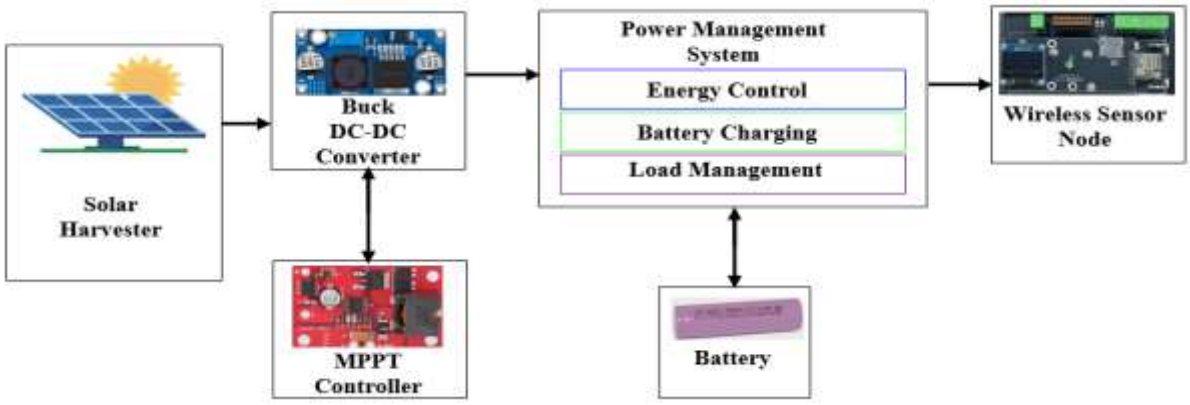


Figure 1: Architecture of the Solar Energy harvester

2.3 Modeling of the Solar Energy Harvesting system

The modeling of the solar energy harvesting system is essential for understanding and predicting the performance of the solar energy harvesting system under varying environmental conditions. This process involves both the mathematical and flowchart model representation of the basic components shown in Figure 1.

2.3.1 Modeling of a Solar Photovoltaic (PV) Panel

The single diode PV model is one of the most widely used and accurate representations of a solar cell's electrical behavior. It captures the essential physical characteristics of a PV device using a simple but effective equivalent circuit that consists of a current source, a diode, and resistive elements as shown in Figure 2 (Salmi *et al.*, 2012).

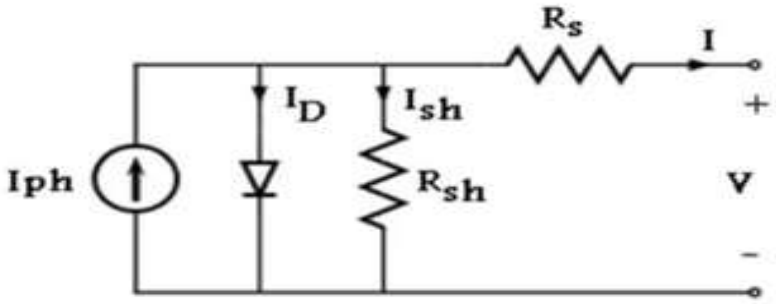


Figure 2: Equivalent circuit of PV cell

Applying Kirchhoff current law to Figure 2, the total photovoltaic current is given by Equation (1) as (Prakash and Sigh, 2016):

$$I = I_{ph} - I_D - I_{sh} \qquad (1)$$

Where, I_{ph} is the photocurrent when the photovoltaic cell is visible to sunlight, I_D is an anti-parallel diode current, and it produces a non-linear response on the photovoltaic cell, and I_{sh} is the current through the shunt resistor.

The diode current I_D is given by Equation (2) as (Himanshu *et al.*, 2018):

$$I_D = I_o[\exp\left(\frac{V+IR_s}{nV_T}\right) - 1] \quad (2)$$

Where, I_o is reverse saturating current due to recombination, V is the PV cell open circuit voltage, I is the solar output current, R_s is the series resistance, n is the diode ideality factor, (1 for ideal, 2 for practical diode), V_T is thee thermal voltage (kT/q), k is the Boltzmann"s constant given as (1.38 x 10^{-23}J/K), T is temperature of solar cell (298 K), q is charge of electrons (1.6 x 10^{-19} C).

The current through the shunt resistance is given by Equation (3) as (Himanshu *et al.*, 2018):

$$I_{sh} = \frac{V+IR_s}{R_{sh}} \quad (3)$$

Substituting the value of I_D, I_{sh} and $V_T = (kT/q)$ in Equation (3.1), we get the complete IV equation for the single solar diode equivalent circuit for which all parameters with output current and voltage is given by Equation (4) as (Prakash and Sigh, 2016):

$$I = I_{ph} - I_o\left[\exp\left(\frac{q(V+IR_s}{nkT}\right) - 1\right] - (\frac{V+IR_s}{R_{sh}}) \quad (4)$$

Where R_{sh} is the shunt resistance and remaining parameter I_o, V, I, R_s, q, n, k, T have already been defined in Equation (2).

The photocurrent of the PV cell depends on the irradiance and the temperature. The photocurrent (I_{sh}) is gives by Equation (5) as (Prakash and Sigh, 2016):

$$I_{ph} = [I_{sc} + K_i(T - 298)] \text{ x } \frac{I_r}{I_{ro}} \quad (5)$$

Where K_i = short-circuit current temperature coefficient of cell = 0.0024, I_{sc} is the short circuit current, and the solar irradiation is represented as I_{ro} = 1000 W/m^2.

The panel saturation current (I_o) is given by Equation (6) as (Prakash and Sigh, 2016):

$$I_O = I_{rs}[\frac{T}{T_r}]^3 \, exp[\frac{q \times E_g}{nk}\left(\frac{1}{T} - \frac{1}{T_r}\right)] \quad (6)$$

Where PV cell reference temperature is given as T_r = 298 K, and I_{rs} is the reverse saturation current.

The band gap energy (E_g), can expressed as Equation (7) as (Premkumar *et al.*, 2020):

$$E_g = E_{go} - \alpha\frac{T^2}{T+\beta} \quad (7)$$

Where E_{go} is the useful energy delivered to the load, α is temperature loss coefficient, β is temperature stabilization constant, T is the temperature of the solar cell.

The modules reverse saturation current (I_{rs}) is given by Equation (8) as (Nguyen and Nguyen, 2015):

$$I_{rs} = \frac{I_{sc}}{exp\left[\frac{q(V+IR_S)}{nKT}\right]-1} \quad (8)$$

Where I_{sc} is the short circuit current and the remaining parameter V, I, R_s, q, n, k, T have already been defined in Equation (3.2).

To enhance the ability of electric power generation from solar PV systems, the solar cells should be implemented in series and parallel combinations. If N_p represents the cells connected in parallel and N_s shows the cells connected in series, the relationship between the output current and voltage is given by Equation (9) as (Chenni *et al.*, 2007; Prakash and Sigh, 2016):

$$I = N_p \times I_{ph} - N_p\, I_o[\exp\,(\frac{{}^{V}/_{N_s} + {}^{IR_s}/_{N_p}}{nV_t})] - I_{sh} \quad (9)$$

$$I_{sh} = \frac{{}^{VN_p}/_{N_s} + IR_s}{R_p} \quad (9)$$

The efficiency (η) of a solar cell is given by Equation (11) as (Himanshu *et al.*, 2018):

$$\eta = \frac{V_{oc} I_{sc} FF}{P_{in}} \quad (10)$$

Where, V_{oc} is the open circuit voltage, I_{sc} is short circuit current on no load, FF is the Fill Factor and P_{in} is the incident optical power.

The Fill Factor (FF) is given by Equation (12) as (Tarak *et al*., 2012; Himanshu *et al.*, 2018):

$$FF = \frac{P_{mas}}{P_{dc}} = \frac{I_m V_m}{I_{sc} V_{oc}} \quad (12)$$

Where, I_m is the maximum current and V_m the maximum voltage of the solar cell.

2.3.1.1 Numerical Solution of the Single-Diode Equation Using Newton–Raphson Method

Applying the single-diode Equation (9), the current I cannot be expressed in terms of the voltage V. To compute the operating point for a given V at each simulation time step, a numerical iterative method is required. The Newton–Raphson method is selected for its quadratic convergence and robustness when provided with a reasonable initial guess, making it the standard choice for solving photovoltaic models.

The method begins by rearranging Equation (4) into a residual function f(I) whose root corresponds to the solution. Setting the equation equal to zero gives Equation (11) as (Chawyuyu *et al*., 2018):

$$f(I_k) = I_{ph} - I_0[\exp(\frac{V+IR_s}{nN_sV_t}) - 1] - (\frac{V+IR_s}{R_{sh}}) - I_k = 0 \quad (11)$$

The Newton–Raphson iteration then approximates the root by linearizing f(I) around the current estimate and solving for the next estimate. This is derived from the first-order Taylor expansion and is given by Equation (12) as (Reis *et al*., 2017):

$$I_{k+1} = I_k - \frac{f(I_k)}{f'(I_k)} \quad (12)$$

where k is the iteration index. The derivative f'(I), which represents the slope of the residual function, is calculated using mathematical expression for efficiency and accuracy using Equation (13):

$$f'(I) = -I_0(\frac{R_s}{nN_sV_t})\exp(\frac{V+IR_s}{nN_sV_t}) - \frac{R_s}{R_{sh}} - 1 \quad (13)$$

An initial guess $I_0 \approx I_{ph}$ (short-circuit current) is used to start the iteration, as it is physically reasonable near the maximum power point under normal operating conditions.

2.3.2 Modeling the Buck DC-DC Converter

The Buck DC-DC converter used because its efficiency is high when compared to Boost DC-DC and Buck-Boost DC-DC Converter (Himanshu *et al.*, 2018). The buck DC-DC converter in the solar energy harvesting system functions to step down the higher voltage output from the photovoltaic panel operating at its maximum power point to a lower stable voltage suitable for charging the battery or powering the wireless sensor node while maintaining high efficiency through switched-mode operation to minimize power losses compared to linear regulators (Baharudin *et al.*, 2018).

This derivation begins from fundamental circuit theory and switching principles analyzing the converter's topology which includes a DC voltage source V_s (from the photovoltaic panel), a controlled switch typically a Metal-Oxide-Semiconductor Field-Effect Transistor (MOSFET), a diode (D), an inductor (L) for energy storage, a capacitor (C) for output filtering and a load as shown in Figure 3 (Jain *et al.*, 2015).

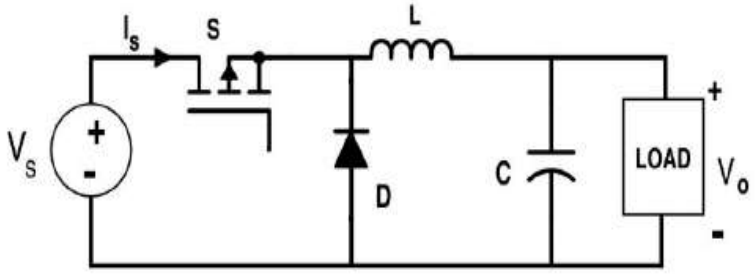


Figure 3: Circuit Model of a Buck DC-DC Converter

The basic operation of the buck converter relies on periodic switching between the ON-state and OFF-state. When the MOSFET switch (S) is at closed position at time t_1, the input voltage appears across the load resistor and when the MOSFET switch remains in the OFF position for time t_2, then the voltage across the load resistor is zero. The Duty Cycle (D) of the buck converter can be varied from 0 to 1 by varying the time period t_1. The Duty Cycle of a buck converter is given by Equation (14) as (Himanshu *et al.*, 2018):

$$D = \frac{V_{out}}{V_{in}} \qquad (14)$$

where V_{in} is the input voltage from the photovoltaic panel typically at the maximum power point and V_{out} is the output voltage set to match the battery nominal.

The inductor current changes in the circuit over time are governed by Faraday's law of induction where the rate of change of current is proportional to applied voltage divided by inductance. Referencing the ON and OFF states from the description leading to Equation (14) the current increase during ON-state is given by Equation (15) as (Himanshu *et al.*, 2018):

$$\Delta I_{L\ on} = \frac{(V_{in} - V_{out})DT}{L} \qquad (15)$$

Where t_{on} = DT, T is the chopping period, L is the inductance, V_{in} is the input voltage, V_{out} is the output voltage from the load.

The current decrease during OFF-state is given by Equation (16) as (Himanshu *et al.*, 2018):

$$\Delta I_{L\ off} = \frac{V_{out}\ (1 - D)T}{L} \qquad (16)$$

Where t_{off} = (1 – D)T.

At Steady State conditions, the energy stored at end of commutation cycle T is equal to the beginning of cycle (Kim *et al.*, 2011). At balance, $\Delta I_{L\ on} = \Delta I_{L\ off}$ in steady state yielding the average inductor current $I_L = I_{out}$ as the output current since the capacitor averages to zero net current. Reusing Equation (14) for D, results in the current ripple Equation (17):

$$\Delta I = \frac{V_{out}(1-D)T}{L} = \frac{V_{out}(1-D)}{fL} \qquad (17)$$

where f = 1/T is the switching frequency in Hertz, L is the inductance in Henry typically chosen so $\Delta I / I_{out} < 0.3$ to limit stress on components.

The output capacitor smooths voltage ripple arising from the discontinuous input current during switching phases derived from charge balance where the capacitor supplies load current during current dips. Building on the ripple from Equation (17), the voltage ripple is approximated under the assumption of triangular current waveform feeding the capacitor given by Equation (18):

$$\Delta V_{out} = \frac{\Delta I}{8fC} \qquad (18)$$

where C is the output capacitance in farads (F) chosen to keep $\Delta V_{out} / V_{out} < 0.01$ for stable supply to the battery or node.

The equivalent input resistance seen by the panel is given by Equation (19) as (Himanshu *et al.*, 2018):

$$R_{in,equiv} = \frac{V_{in}}{I_{in}} = \frac{R_{load}}{D^2} \quad (19)$$

allowing duty modulation to tune $R_{in,equiv}$ to the maximum power point resistance typically 3 to 5 ohms for small panels enhancing energy extraction efficiency. The complete power output from the buck in the harvesting chain is the managed power delivered to subsequent stages and is given by Equation (20) as:

$$P_{conv} = \eta_{buck} P_{mpp} \quad (20)$$

where P_{mpp} is the panel maximum power and η_{buck} is the efficiency of the buck converter.

2.3.3 Modeling of the Maximum Power Point Tracking (MPPT)

The maximum power point techniques are widely used in the design of PV solar systems to maximum power extraction from the solar radiation under varying conditions. It is an algorithm that continuously measures the voltage (V*pv*) and current (I*pv*) from the PV panel and calculate the amount of duty cycle (D) to be fed to the MOSFET switch of the converter (Himanshu *et al.*, 2018).

The P and O techniques Is mostly used in solar energy harvesting system (Himanshu *et al.*, 2018). The P and O algorithm uses the principle of impedance matching between the solar panel and the load. For maximum power transfer between the panel and load, impedance matching is very necessary. By using a DC-DC buck converter, the impedance is matched by changing the duty cycle (ΔD) of the MOSFET switch. The input voltage (V_{in}), output voltage (V_{out}) and duty cycle are related by Equation (14) and (19).

If the duty cycle changes (ΔD), then the solar harvester output voltage (V_{out}) changes. If the duty cycle (D) is increased, the solar harvester output voltage (V_{out}) also increases. By changing the duty cycle (D), the impedance of the load resistance (R_L) can be matched with the solar harvester input impedance for maximum power transfer to the load for optimal performance.

The steps procedure in the P and O algorithm is shown in Figure 4 (Dan *et al*., 2014).

3. RESULTS AND DISCUSSION

This section presents a detailed analysis of the MATLAB/Simulink simulation results for the proposed solar energy harvesting system focusing on solar irradiance variation, energy generation, and system performance. The findings are discussed in relation to system efficiency, reliability, and overall energy availability under varying environmental conditions.

3.1 Daily solar Irradiance Profiles (All Months)

The daily solar irradiance profiles across all months Figure 6, exhibit a consistent pattern characterized by a gradual increase from sunrise (approximately 06:20 hours), reaching peak values between 12:00 noon and 2:00 pm, and subsequently declining towards sunset. Peak irradiance values range between 400 W/m² and 550 W/m², with the highest intensities observed during the late dry season months (February - March) and early dry season (November - December).

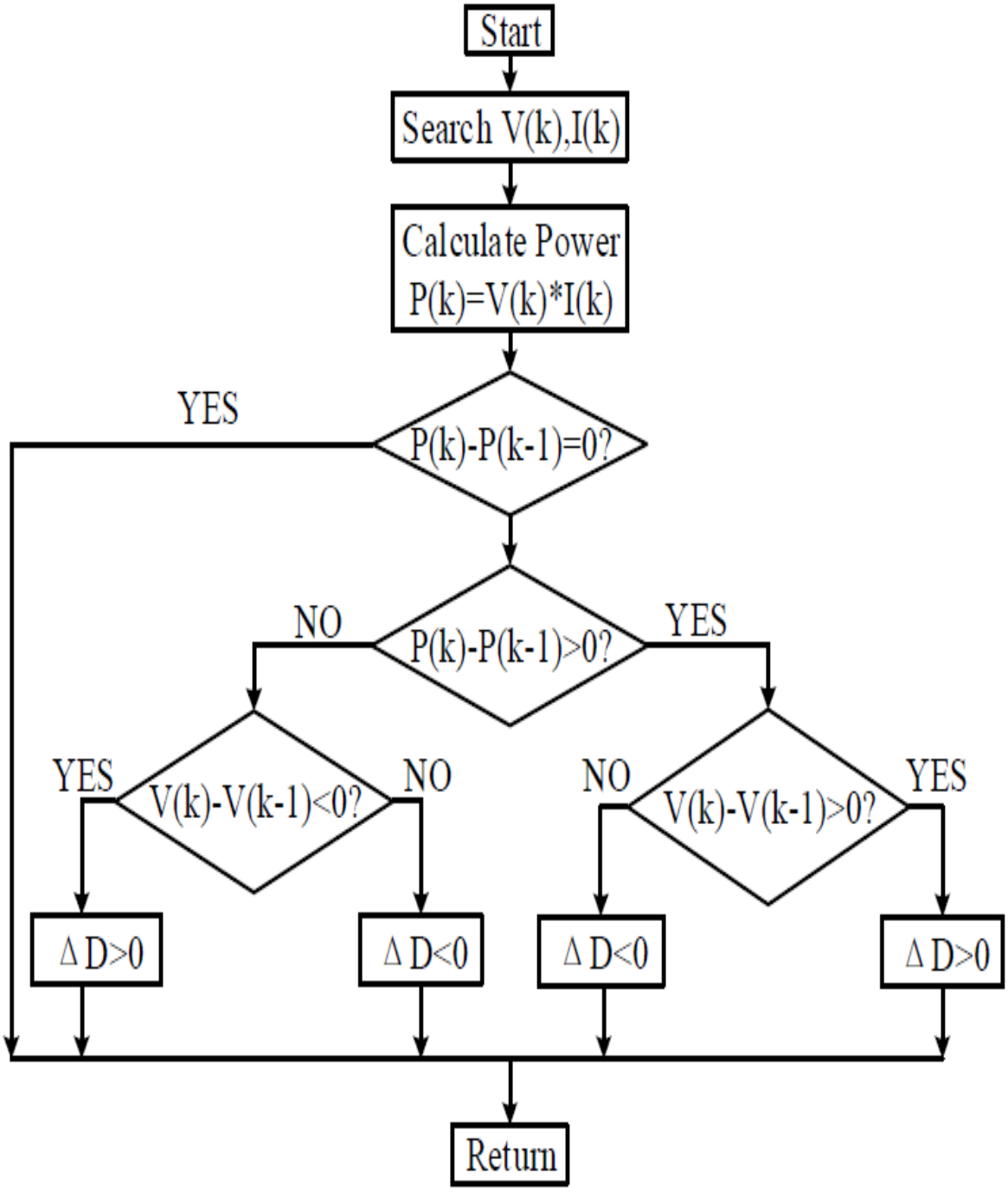


Figure 4: Perturbation and Observation Algorithm

On the other hand, reduced peak values are evident during the rainy season months (June - September), attributable to increased cloud cover and atmospheric attenuation. The smooth bell-shaped distribution confirms the reliability of the dataset and reflects typical tropical solar radiation behavior, validating its suitability for energy harvesting system modeling.

3.2 Monthly Average Solar Irradiance with Variability Range

The monthly average solar irradiance Figure 7, demonstrates clear seasonal variation, with values ranging from approximately 70 W/m² to 140 W/m².

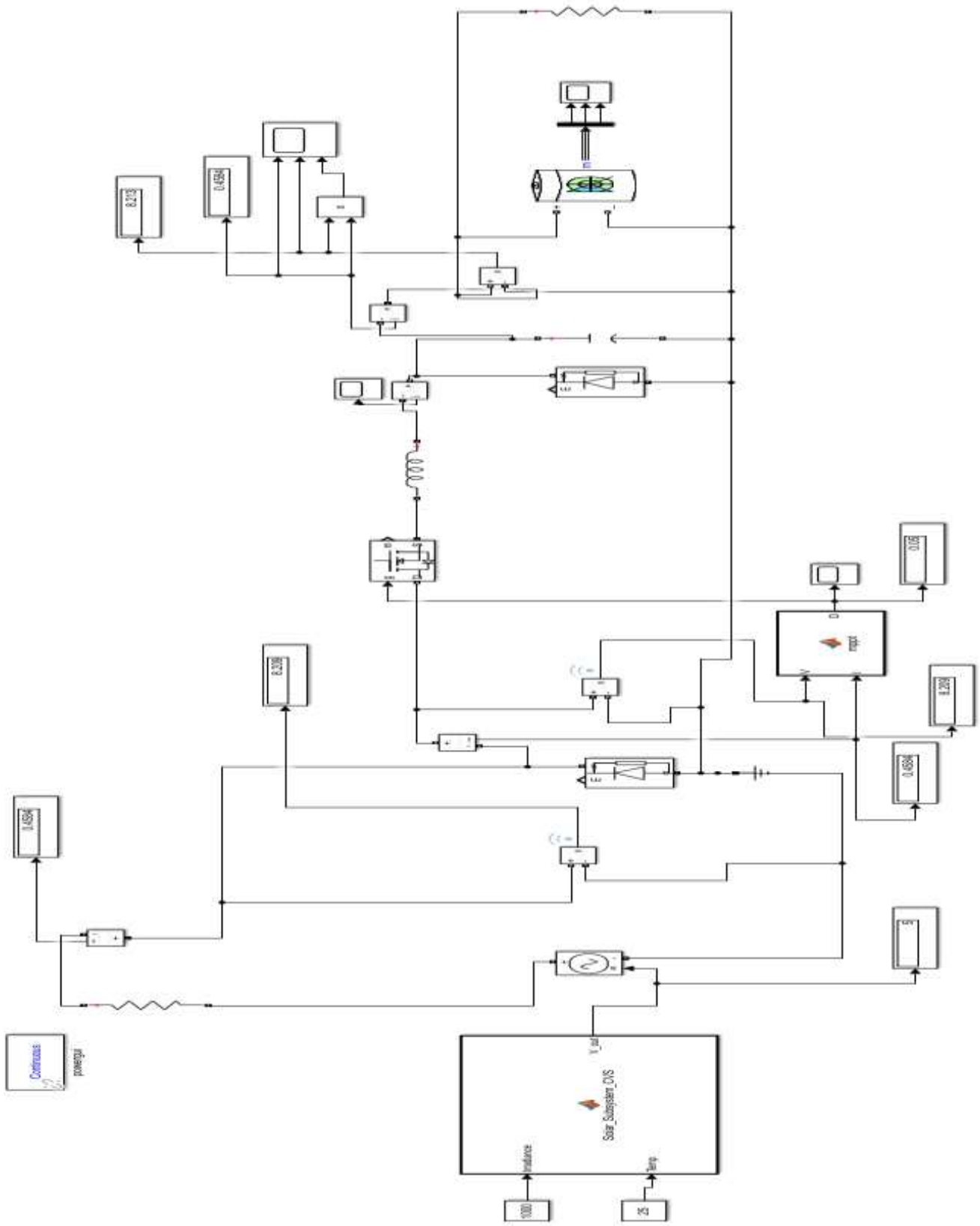


Figure 5: Simulink model of the Solar Energy Harvesting System.

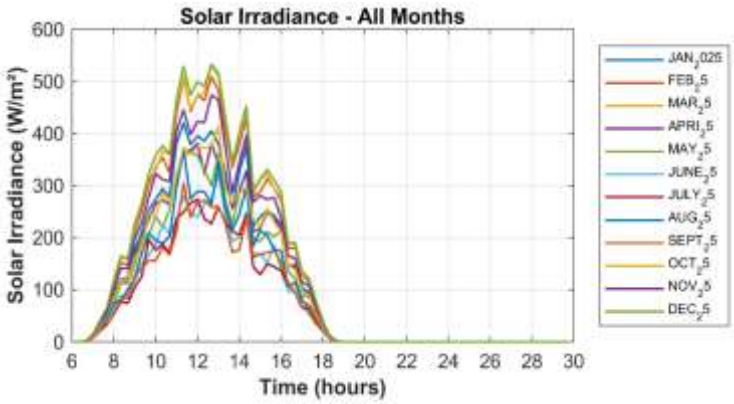


Figure 6: Solar Irradiance all Months

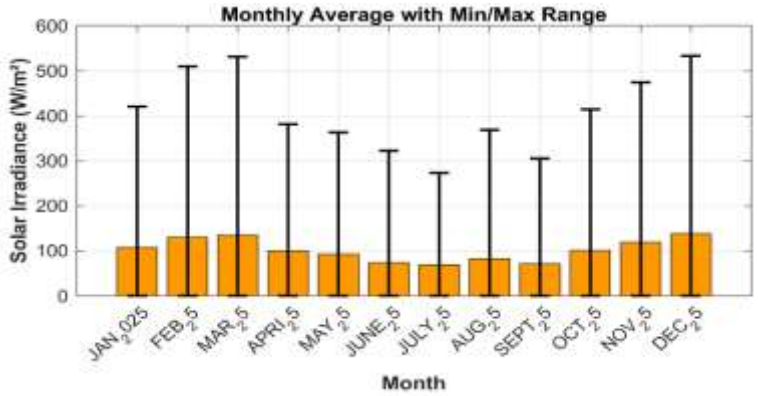


Figure 7: Monthly Average with Min/Max Range

The highest averages occur in February, March, and December, while the lowest values are recorded during June, July, and September, corresponding to the peak of the rainy season. The large min/max error bars indicate a noticeable daily variation, especially during transitional months, highlighting the intermittency of solar energy. This variability has important implications for system design, particularly in sizing storage elements and ensuring reliable power supply during low irradiance periods.

3.3 Solar Irradiance Heatmap Analysis

The heatmap Figure 8, provides a comprehensive visualization of irradiance distribution across both time and months. High-intensity regions are concentrated around midday (time points corresponding to 12:00 noon - 2:00 pm, particularly in February, March, November, and December.

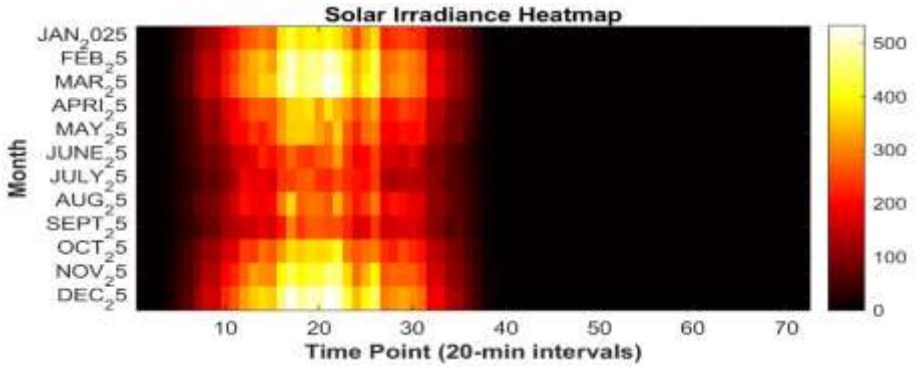


Figure 8: Solar Irradiance Heat Map.

In contrast, the rainy season months display a noticeable reduction in intensity and spread of high irradiance zones. The heatmap clearly illustrates the temporal concentration of solar energy, emphasizing that effective energy harvesting is largely confined to a limited window within the day.

3.4 Monthly Trends of Solar Irradiance (Average, Maximum, Minimum)

The monthly trend analysis Figure 9 further confirms the seasonal behavior of solar irradiance. The maximum irradiance peaks at approximately 530 - 540 W/m² in March and December, while the minimum values remain close to zero across all months due to nighttime conditions.



Figure 9: Monthly Trends

The average irradiance follows a similar trend, peaking in the dry season and dipping during the rainy season. This repeated variation highlights the strong dependence of solar energy availability on climatic conditions, which must be accounted for in long-term system performance evaluation.

3.5 DC-DC Converter Output Performance

The DC-DC converter output Figure 10, closely mirrors the solar irradiance pattern, indicating effective energy conversion. The maximum output power reaches approximately 850 - 870 mW during high irradiance months March and December, while lower outputs are observed during the rainy season approximately 450 - 600 mW.

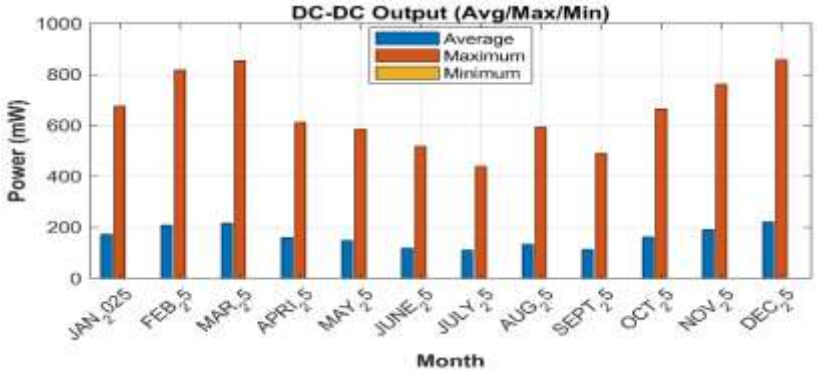


Figure 10: DC-DC Converter Output

The average output remains relatively stable but reflects seasonal dips. This demonstrates that the converter operates efficiently across varying input conditions, though its performance is inherently limited by the available solar resource.

3.6 Power Management System (PMS) Output Performance

The PMS output Figure 11, shows a regulated and slightly reduced power profile compared to the DC-DC converter output, reflecting system losses and control actions. Maximum PMS output reaches approximately 780 - 800 mW, while

minimum values remain consistent across months. The PMS effectively smoothens fluctuations and ensures stable power delivery to the load, demonstrating its critical role in maintaining system reliability despite variability in harvested energy.

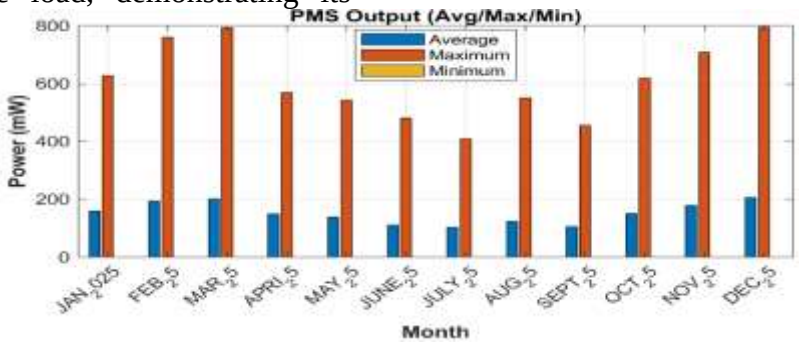


Figure 11: PMS Output

3.7 Load Power Consumption Characteristics

The load power profile Figure 12, indicates a demand range of approximately 400 - 750 mW, with average consumption varying between 100 mW and 200 mW. The load demand remains relatively stable compared to the supply variations, highlighting the importance of energy storage and power management in ensuring continuous operation. The mismatch between peak generation and load demand further emphasizes the need for efficient energy buffering mechanisms.



Figure 12: Load Power

3.8 Best (December) vs Worst (July) Month Performance

The comparative analysis between December (best) and July (worst) month clearly highlights the strong dependence of the solar energy harvesting system on solar resource availability. From the graph, December exhibits significantly higher solar irradiance approximately 135 - 140 W/m² compared to July approximately 65 - 70 W/m², representing nearly a two times increase. This seasonal variation is consistent with the dry season in the Niger Delta region, where clearer skies in December enhance solar energy availability, while increased cloud cover during July the rainy season reduces irradiance level.

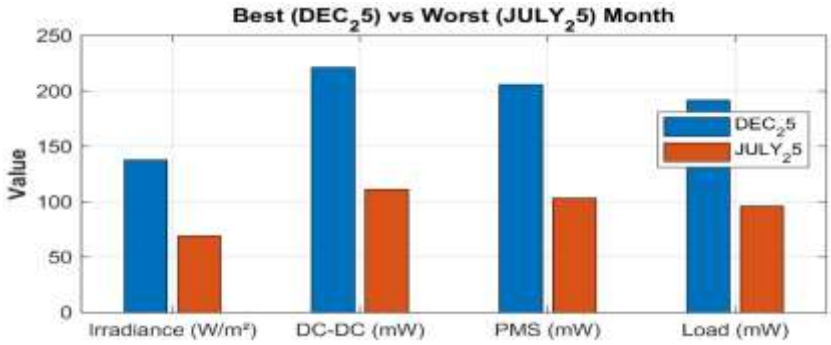


Figure 13: Best Month (December 20) vs Worst Month (July 25)

3.9 Energy Output and System Efficiency

The energy output analysis reveals that daily harvested energy ranges from approximately 2.3 Wh to 4.6 Wh, with peak values occurring during March and December, and minimum values during July and September. The system efficiency remains relatively constant at approximately 7.15%, indicating stable conversion performance despite fluctuations in input energy. This consistency suggests that system losses are well-managed and that performance variations are primarily driven by environmental conditions rather than inefficiencies in system design.

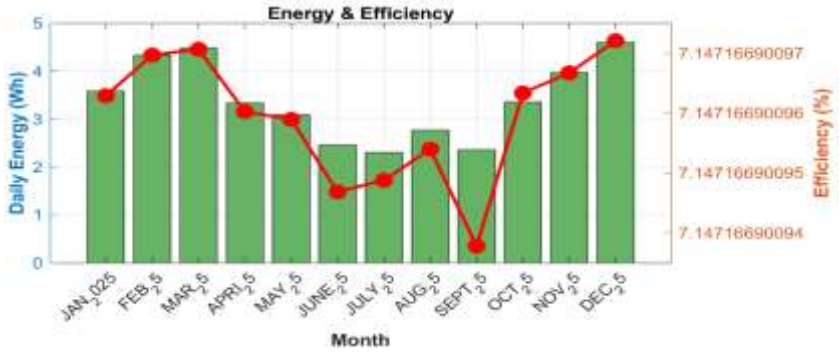


Figure 13: Energy and Efficiency

The results collectively demonstrate that solar energy availability in the study location exhibits strong daily and seasonal variations. While high potential exists during dry season months, significant reductions during the rainy season necessitate robust energy storage and intelligent power management strategies. The close alignment between irradiance, converter output, and PMS output validates the effectiveness of the system design. However, the observed variability underscores the importance of hybridization with other energy sources (such as RF and wind) to ensure continuous system autonomy and reliability.

4. CONCLUSION

This study presents the modeling and comprehensive performance evaluation of a proposed solar energy harvesting system using MATLAB/Simulink simulations under varying conditions. The system architecture, consisting of a photovoltaic (PV) source, DC–DC converter, maximum power point tracker, power management system, storage and a wireless sensor node, was assessed through monthly comparative and solar irradiance analyses.

The results demonstrated a strong dependence of harvested energy on seasonal solar irradiance. Peak performance was recorded during high-irradiance months, with daily harvested energy reaching approximately 4.6 Wh/day, while minimum output during low-irradiance months ranged between 2.3 - 2.5 Wh/day. Seasonal combination further confirmed that late-year periods provide the highest energy yield, whereas mid-year months provide the lower energy yield.

Despite substantial variation in harvested energy, the overall system efficiency remained nearly constant at approximately 7.15% throughout the year. This stability confirms robust DC–DC converter operation, effective power regulation, and minimal sensitivity of conversion efficiency to environmental fluctuations. The proportional relationship between irradiance, converter output, PMS output, and load power further validates the scalability and predictable behavior of the system.

Overall, the findings confirm that the proposed solar energy harvesting system is environmentally adaptive, electrically stable, and capable of reliable year-round operation. Its consistent efficiency and predictable seasonal scaling make it suitable for low power standalone applications, particularly in regions experiencing significant seasonal solar variability.

REFERENCES

Abd Aziz, A., Sekercioglu, Y.A., Fitzpatrick, P. and Ivanovich, M. (2012). A survey on distributed topology control techniques for extending the lifetime of battery powered wireless sensor networks. *IEEE Communications Surveys* and *Tutorials, 15*, 121–144.

Ahmad, I., Rehman, M. M. U., Khan, M., Abbas A., Ishfaq, S. and Malik, S. (2019). Flow-Based Electromagnetic-Type Energy Harvester using Microplanar Coil for IoT Sensors Application. *International Journal of Energy Research, 43(10)*, 5384–5391.

Baharudin, N. H., Mansur, T. M. N. T., Hamid, F. A, Ali, R. and Misrun, M. I. (2018). PerformanceAnalysis of DC-DC Buck Converter for Renewable Energy Applications. *Journal of Physics: Conference Series, 1019(1)*, 1-7.

Chawyuyu, K., Panhathai, B., Apirat, S. and Rongrit, C. (2018). Simulation and Experimental Results for a Single Diode Photovoltaic Model using Newton-Raphson Parameter Estimation Method. *Mahasarakham International Journal of Engineering Technology, 4(2)*, 29-36.

Chenni, R., Makhlouf, M., Kerbache, T. and Bouzid, A. (2007). A detailed modeling method for photovoltaic cells. *Energy, 32(9)*, 1724-1730.

Choudhary, P., Bhargava, L., Singh, V., Choudhary, M. and Suhag, A. K. (2020). A survey – Energy harvesting sources and techniques for internet of things devices. *Materials Today, 30(1)*, 52-56.

Diaz, M., Martin, C. and Rubio, B. (2016). State-of -the-art, challenges, and open issues in the integration of Internet of Things and cloud computing. *Journal of Network and Computer Applications*, 67, 99-117.

Divyanshu, S., Aditya, P. S., Seema, M. and Deepti, G. (2024). Advancements and Challenges in wireless sensor Networks: A Comprehensive review. *International Journal of Research, Publication and Reviews*, *5(6)*, 836-842.

Fadoua, Y. and Adil, K. (2022). *Energy Harvesting in wireless communication: A survey.* Paper presented at the 2021 International Conference on Energy and Green Computing, Mekness, Morocco. Retrieved from https://doi.org/10.1051/e3sconf/202233600074.

Gubbi, J., Buyya, R., Marusic, S. and Palaniswami, M. (2013). Internet of Thints (IoT): A vision, architectural elements, and future directions. *Future Generation Computer Systems, 29(7)*, 1645-1660.

Himanshu, S., Madhav, S., Chetan, S, Ahteshamul, H. and Zainul, A. J.

(2018). *Performance Analysis of a Solar Powered DC-DC Buck Converter for Energy Harvesting IoT Nodes.* Paper presented at the 2018 3rd International Innovative Applications of Computational Intelligence on Power, Energy and Controls with their Impact on Humanity (CIPECH), Ghaziabad, India. Retrieved from https://ieeexplore.ieee.org/document/8724183.

Hussain, M. N., Halim, M. A., Ali-Khan, M. Y., Ibrahim, S. and Haque, A. (2024). A Comprehensive Review on Techniques and Challenges of Energy Harvesting from Distributed Renewable Energy Sources for Wireless Sensor Networks. *Control Systems and Optimization Letters*, 2(1), 15-22.

Iftikhar, A., Lim, M. H., Ahmad, M. A., Syed, A. I. and Leong, M. S. (2021). Scopes, challenges and approaches of energy harvesting for wireless sensor nodes in machine condition monitoring systems: A review. *Measurements,183*, 1-13.

Jaehoon, C., Inki. J. and Chong-Yun, K. (2019). A Brief review of sound energy harvesting. *Nano Energy, 56*, 169-183.

Jain, P. K., Nirmal, and Kumar, A. (2015). *Interleaved DC to DC Buck Converter for Low Power Application.* Paper presented at the 2015 International Conference on Energy, Power and Environment: Towards Sustainable Growth (ICEPE), Shillong, India. Retrieved from https://ieeexplore.ieee.org/document/7510110.

Jaspreet, S., Ranjit, K. and Damanpreet, S. (2020). Energy Harvesting in Wireless Sensor Networks: A Taxonomic Survey. *International Journal of Energy Research, 45(1),* 1-23.

Katrina, C., Diana, S. N. M. and Nasir, B. R. H. (2021). Low power energy harvesting systems: State of the art and future challenges. *Renewable and Sustainable Energy Reviews,147*, 1-20.

Keh, H. C., Wang, Y. H., Lin, K. Y. and Lin, C. C. (2011). Power saving mechanism with optimal sleep control in wireless sensor networks. *Tamkang Journal of Science and Technology*, 14(3), 235–243.

Kim, J., Kim, J. and Kim, C. (2011). A regulated charge pump with a low power integrated optimum power point tracking algorithm for indoor solar energy harvesting. *IEEE Transactions on Circuits and Systems II: Express Briefs, 58(12),* 802–806.

Li, S. E., Li, G., Yu, J., Liu, C., Cheng, B., Wang, J. and Li, K. (2018). Kalman filter-based tracking of moving objects using linear ultrasonic sensor array for road vehicles. *Mechanical Systems and Signal Processing, 98,* 173-189.

Marco, G. (2021). Energy Harvesting Strategies for Wireless Sensor Networks and Mobile Devices: A Review. *Electronics*, 10(6), 1-53.

Muhammad, U. M., Hein, V., Avinash, S. and Muhammad, O. (2025). Advances in Energy Harvesting for Sustainable Wireless Sensor Networks: Challenges and Opportunities. *Hardware, 5(1)*, 1-26.

Nguyen, X.H. and Nguyen, M.P. (2015). Mathematical modeling of photovoltaic cell/module/arrays with tags in Matlab/Simulink. *Environmental Systems Research, 4*,1-13.

Panatik, K. Z., Kamardin, K., Shariff, S. A., Yuhaniz, S. S., Ahmad, N. A., Yusop, O. M. and Ismail, S. (2016). *Energy harvesting in wireless sensor networks: A survey*. Paper presented

at *IEEE 3rd International Symposium on Telecommunication Technologies*, Kuala Lumpur, Malaysia. Retrieved from https://ieeexplore.ieee.org/document/7918084.

Penella, M. T., Albesa, J. and Gasulla, M. (2009). *Powering Wireless Sensor Nodes: Primary Batteries versus Energy Harvesting*. Paper presented at the 2009 IEEE instrumentation and measurement technology conference, Singapore. Retrieved from https://www.researchgate.net/publication/41821038_Powering_wireless_sensor_nodesPrimary_batteries_versus_energy_harvesting.

Prakash, R. and Singh, S. (2016). Designing and modelling of solar photovoltaic cell and array. *IOSR Journal of Electrical and Electronics Engineering, 11(2)*, 35-40.

Prauzek, M., Konecny, J., Borova, M., Janosova, K., Hlavica, J. and Musilek, P. (2018). Energy harvesting sources, storage devices and system topologies for environmental wireless sensor networks: A review. *Sensors*,18(8),1-22.

Premkumar, M., Chandrasekaran, K. and Sowmya, R. (2020). Mathematical modelling of solar photovoltaic cell/panel/array based on the physical manufacturer's parameters datasheet. *International Journal of Renewable energy development, 9(1),* 7-22.

Ramakrishnan, M., Rajan, G., Semenova, Y. and Farrell, G. (2016). Overview of fiber optic sensor technologies for strain/temperature sensing applications in composite materials. *Sensor, 16(1),* 1-27

Raquib, M. F., Ahmed, W. R. and Muhammad, F. S. (2016). Renewable energy harvesting for wireless sensors using passive RFID tag technology: A review. *Renewable and Sustainable Energy Reviews, 58,* 1114-1128.

Ray, P. P. (2018). A survey on internet of Things architecture. *Journal of King Saud University – Computer and Information Science, 30(3),* 291-319.

Reis, L. R. D., Camacho, J. R. D. and Novacki, F. (2017). The Newton Raphson Method in the Extraction of Parameters of PV Modules. *Renewable Energy and Power Quality Journal, 1(15),* 634-639.

Salmi, T., Bouzguenda, M., Gastli, A. and Masmoudi, A. (2012). Matlab/simulink based modeling of photovoltaic cell. *International journal of renewable energy research, 2(2)*, 213-218.

Servent, A., Daskalakis, S., Collado, A. and Georgiadis, A. (2017). *A proximity wireless sensor based on backscatter communication.* Proceedings of the 2017 International Computational Electromagnetics Society Symposium, Italy. Retrieved from https://www.daskalakispiros.com/files/2017_aces_Georgiadis.pdf.

Shaikh, F. K., Zeadally, S. and Exposito, E. (2015). Enabling technologies for green internet of things. *IEEE System Journal, 11(2),* 983–994.

Sichitiu, M. L. and Dutta, R. (2005). *Benefits of multiple battery levels for the lifetime of large wireless sensor networks*. Paper presented at the 4th International IFIP-TC6 Conference on Research in Networking, Waterloo, Canada. Retrieved from https://dl.ifip.org/db/conf/networking/networking2005/SichitiuD05.pdf.

Song, Y. G., Shim, Y. S., Kim, S., Han, S. D., Moon, H. G., Noh, M. S., Lee, K., Lee, H. R., Kim, J. S., Ju, B. K. and Kang, C. Y. (2017). Downsizing gas sensors based on semiconducting metal oxide: Effects of electrodes on gas sensing properties. *Sensors and Actuators B: Chemical, 28*, 949-956.

Tarak, S., Mounir, B., Adel, G. and Ahmed, M. (2012). MATLAB/Simulink Based Modelling of Solar Photovoltaic Cell. *International Journal of Renewable Energy Research, 2(2)*, 213-218.

Tiliute, D. E. (2007). Battery management in wireless sensor networks. *Elektronika Ir Elektrotechnika*, *76(4)*, 9–12.

Wang, J., Gao, Y., Liu, W., Sangaiah, A.K. and Kim, H. J. (2019). Energy efficient routing algorithm with mobile sink support for wireless sensor networks. Sensors, 19(7), 1-19.

Yamazoe, N. (2005). Toward innovations of gas sensor technology. *Sensors and Actuators B: Chemical, 108(1-2)*, 2-14.

Zhou, P., Wang, C. and Yang, Y. (2019). *Self-sustainable sensor networks with multi-source energy harvesting and wireless charging*. Paper presented at the 2019 IEEE International Conference on Computer communications, Paris, France. Retrieved from https://www.researchgate.net/publication/333849744_Self-sustainable_Sensor_Networks_with_Multi-source_Energy_Harvesting_and_Wireless_Charging.